Compact high order finite volume method on unstructured grids I: Basic formulations and one-dimensional schemes

Article *in* Journal of Computational Physics · February 2016

DOI: 10.1016/j.jcp.2016.01.036

CITATIONS
24

READS
558

3 authors:

Qian Wang
École Polytechnique Fédérale de Lausanne
19 PUBLICATIONS **356** CITATIONS
SEE PROFILE

Yu-Xin Ren
Tsinghua University
87 PUBLICATIONS **1,134** CITATIONS
SEE PROFILE

Wanai Li
Sun Yat-Sen University
26 PUBLICATIONS **336** CITATIONS
SEE PROFILE

Compact high order finite volume method on unstructured grids I: basic formulations and one-dimensional schemes

Qian Wang[1], Yu-Xin Ren[1], Wanai Li[2]

[1] Department of Engineering Mechanics, Tsinghua University, Beijing 100084, China

[2]Sino-French Institute of Nuclear Engineering & Technology, Sun Yat-Sen University, Zhuhai 519082, China

Corresponding author: ryx@tsinghua.edu.cn (Yu-Xin Ren)

Abstract:

The large reconstruction stencil has been the major bottleneck problem in developing high order finite volume schemes on unstructured grids. This paper presents a compact reconstruction procedure for arbitrarily high order finite volume method on unstructured grids to overcome this shortcoming. In this procedure, a set of constitutive relations are constructed by requiring the reconstruction polynomial and its derivatives on the control volume of interest to conserve their averages on face-neighboring cells. These relations result in an over-determined linear equation system, which, in the sense of least-squares, can be reduced to a block-tridiagonal system in the one-dimensional case. The one-dimensional formulations of the reconstruction are discussed in detail and a Fourier analysis is presented to study the

dispersion/dissipation and stability properties. The WBAP limiter based on the secondary reconstruction is used to suppress the non-physical oscillations near discontinuities while achieve high order accuracy in smooth regions of the solution. Numerical results demonstrate the method's high order accuracy, robustness and shock capturing capability.

Keywords: Compact reconstruction, High order, Finite volume method, Shock capturing.

1 Introduction

High order numerical methods on unstructured grids are one of the active research areas in computational fluid dynamics (CFD). Such methods are believed to have the advantages of high order accuracy, low dissipation/dispersion, and capability of handling both complex physics and geometries. Therefore, in applications such as direct numerical simulation (DNS) and large eddy simulation (LES) of turbulent flows and computational aeroacoustics (CAA), high order methods have significant potential to achieve higher efficiency in terms of number of elements required to accurately resolve important flow features than typical second order schemes [1]. High order methods on unstructured grids are widely considered as the next major breakthrough in CFD. Over the last two decades, various high order methods have been developed, such as the high order *k*-exact [2-5]/ WENO [6-9] finite volume (FV) schemes, discontinuous Galerkin (DG) method [10-14], P_NP_M procedure [15-17], Residual Distribution (RD) method [18-21], spectral volume (SV) [22-25]/ spectral difference (SD) [26-28] methods and correction procedure via reconstruction (CPR) method [29, 30].

The motivation of the present paper is to design a FV scheme that overcomes some important drawbacks associated with the high order FV schemes. The high order FV schemes are briefly reviewed before presenting the basic ideas of the present method. The key ingredient of the FV methods to achieve high order accuracy is the high order representation of physical data inside the cell. One of the pioneering works in this area is the FV scheme based on the *k*-exact reconstruction, which was first proposed by Barth and Fredrichson [2] on 2D grids and later generalized to 3D grids by Delanaye and Liu [3]. Further development of this scheme was made by Ollivier-Gooch [4, 5] and others. The ENO and WENO schemes were firstly developed on structured grids [31-39]. The ENO scheme on unstructured grids was developed by Abgrall [40] and the WENO scheme on unstructured grids was developed by Friedrich [6]. These schemes were further studied by Dumbser [7, 8] and Shu [9] to improve their efficiency and accuracy. Li and Ren [41] proposed an improved WENO scheme on unstructured grids using the secondary reconstruction (SR). The basic idea of the SR is to use the continuations of the *k*-exact reconstructions on neighboring cells as the additional candidate reconstructions for the current cell. The polynomials of the SRs are derived analytically and are very simple, which makes the improved WENO scheme being much more efficient than the traditional WENO schemes.

The number of cells in the stencil of a high order FV scheme is usually large because the reconstruction in FV methods uses only the cell averages on the corresponding stencil. Furthermore, the reconstruction procedure for the high order FV schemes could be singular especially on unstructured grids. To overcome this problem, the reconstruction is sometimes

performed in the least-squares sense, for which even larger stencil is needed. The large stencil results in a series of problems [21, 42]. The first one is cache missing due to the data in the stencil being far away in memory. The second one is that large amount of data need to be transferred at the interface of two partitions in parallel computing, which leads to the deterioration of the parallel efficiency. The third one is that on a larger stencil, more memory is needed to store the coefficients associated with the cells in the stencil. Therefore, very large stencil has been one of the most serious problems for the high order FV schemes. In fact, one of the important motivations to develop the high order schemes with internal degree of freedom (DOF) such as the DG and SV/SD schemes is to reduce the size of the stencil so that the stencil is compact and independent of the order of accuracy.

This paper presents a compact least-squares (CLS) reconstruction procedure for high order FV method. The key novelty of this procedure is that it can achieve arbitrarily high order accuracy using a compact stencil consisting of only the face-neighboring cells. To explain the basic idea of this reconstruction, we note that the polynomial of a traditional reconstruction procedure is determined by conserving the cell averages of the solution on the current cell as well as on the neighboring cells belonging to the stencil of the reconstruction for sufficiently smooth solution. Since the number of unknowns in the reconstruction polynomial increases very fast with the degree of the polynomial, a very large stencil is required for high order polynomial reconstruction. To cure this shortcoming and maintain the compact stencil for arbitrarily high order reconstruction, the present reconstruction procedure requires not only the dependent variables but also its various orders of derivatives to conserve their means on

the face-neighboring cells. The conservation of the averages of the various orders of derivatives provides additional constitutive relations so that the reconstruction can be performed on a compact stencil. In practice, the number of all the constitutive relations is always larger than the unknowns in the reconstruction polynomial. Therefore, the constitutive relations result in an over-determined linear equation system, which, in the sense of least-squares, can be reduced to a block-tridiagonal linear equation system in one-dimensional cases. In multi-dimensional cases, this reconstruction procedure is more complicated and a proper iteration method is needed to perform the reconstruction. Because the reconstruction procedure is new, it deserves a detail study on its property and performance, which is easier to carry out in one-dimensional case. Therefore, only the one-dimensional conservation law is considered in the present paper. The extension of the present method to multi-dimensional cases will be presented in a forthcoming paper in which an efficient procedure for solving the multi-dimensional reconstruction problem on unstructured grids will be proposed.

The remainder of this paper is organized as follows. In Section 2, the basic idea and basic formulations of the CLS reconstruction are presented in detail. A Fourier analysis is performed to study the dispersion/dissipation and stability properties of the reconstruction. In section 3, the reconstruction is applied to the FV schemes for solving one-dimensional Euler equations. The rest of this section presents the slope limiter for shock capturing calculation and an efficient limiting procedure in characteristic space. The numerical examples are presented in Section 4 to validate the performance of the proposed FV method and the concluding remarks are given in Section 5.

2 The compact least-squares reconstruction

2.1 The reconstruction procedure

This subsection describes the basic idea and basic formulations of the proposed reconstruction procedure. For convenience, some notation is defined as follows.

$I_i \equiv \left[x_{i-1/2}, x_{i+1/2}\right]$ is the *i*-th control volume. The control volumes are generated through a non-overlapping partition of the computational domain Ω with $\Omega = \bigcup_{i=1}^{N} I_i$. $\Delta x_i = x_{i+1/2} - x_{i-1/2}$ is the length of I_i and $x_i = \left(x_{i+1/2} + x_{i-1/2}\right)/2$ is the centroid of I_i. $\overline{u}_i = \dfrac{1}{\Delta x_i}\int_{I_i} u\,dx$ is the cell average of the dependent variable u on I_i.

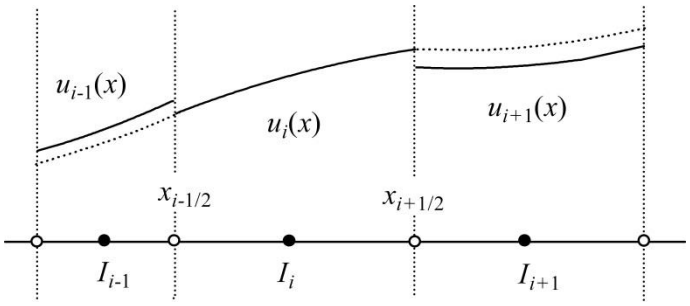

Fig. 1. Grid stencil in one-dimension.

Mathematically, the reconstruction problem in the FV scheme can be stated as follows. Given the cell average

$$\overline{u}_j = \frac{1}{\Delta x_j}\int_{I_j} u(x)\,dx \tag{1}$$

of a solution $u(x)$ on every control volume $I_j \in \Omega$, a degree *k* polynomial

$$u_i(x) = \bar{u}_i + \sum_{l=1}^{k} u_i^l \varphi_{l,i}(x) \tag{2}$$

is constructed to approximate the solution on $I_i \in \Omega$, where $u_i^l = \frac{1}{l!}\frac{\partial^l u}{\partial x^l}\left(\Delta x_i\right)^l$ is the unknown reconstruction coefficient to be determined and $\varphi_{l,i}\left(x\right)$ is the zero-mean basis defined by

$$\varphi_{l,i}\left(x\right) = \left(\delta x_i\right)^l - \frac{1}{\Delta x_i}\int_{I_i}\left(\delta x_i\right)^l dx, \ \ \delta x_i = \left(x - x_i\right)/\Delta x_i .$$

The basis presented above is normalized by the length of the cell to avoid growth of the condition number of the reconstruction matrix with grid refinement [6, 40]. Because of the use of the zero-mean basis, the reconstruction polynomial $u_i\left(x\right)$ is always conservative in the sense

$$\frac{1}{\Delta x_i}\int_{I_i} u_i(x)dx = \bar{u}_i .$$

There are *k* unknowns $u_i^l, \ l = 1, 2, \cdots, k$ in Eq. (2) to be determined in the reconstruction procedure.

The traditional reconstruction algorithms (such as the *k*-exact, ENO and WENO reconstructions) for FV schemes determine the unknowns $u_i^l, l = 1, 2, \cdots, k$ by conserving the cell averages of the solution on the neighboring cells of I_i belonging to the stencil of the reconstruction for sufficiently smooth solutions. More specifically, on the stencil S_i which consists of $n_i \geq k$ neighboring cells of I_i and $I_i \notin S_i$, it is required that

$$\frac{1}{\Delta x_j}\int_{I_j} u_i(x)\, dx = \bar{u}_i + \sum_{l=1}^{k} u_i^l \left(\frac{1}{\Delta x_j}\int_{I_j} \varphi_{l,i}(x)\, dx \right) = \bar{u}_j \tag{3}$$

for all $I_j \in S_i$. This procedure results in a system of n_i linear equations. If $n_i > k$, the

system of equations is over-determined and needs to be solved using the least-squares methods. The main problem of this approach is that the number of cells in the stencil S_i increases with k. This will lead to a large stencil for high order FV schemes. For multi-dimensional problems, the number of unknowns in the reconstruction polynomial increases even faster with the degree of the polynomial. Large stencils in high order FV schemes destroy the compactness of the schemes and reduce the computational efficiency especially for parallel computing, which has been a bottleneck problem for high order FV methods on unstructured grids.

To solve this problem, this paper presents a compact reconstruction procedure which is compact in the sense that the stencil only consists of the face-neighboring cells for arbitrarily high order FV method. In this paper, only the one-dimensional conservation law is studied to reveal some basic properties of this reconstruction procedure. Extension of the present reconstruction procedure to multi-dimensional cases will be presented in forthcoming papers.

The basic idea of the proposed reconstruction is as follows. Besides the constitutive relations described by Eq. (3), additional constitutive relations are supplied by requiring that the cell averages of various orders of derivatives of the reconstruction polynomial are conserved on S_i. Namely, for all $I_j \in S_i$,

$$\frac{1}{\Delta x_j}\int_{I_j} \frac{\partial^m u_i(x)}{\partial x^m}\,dx = \frac{1}{\Delta x_j}\int_{I_j} \frac{\partial^m u_j(x)}{\partial x^m}\,dx,\ 0 \le m \le M \tag{4}$$

where $M \le k$. Substituting Eq. (2) into Eq. (4), we obtain

$$\sum_{l=1}^{k} u_i^l \left(\frac{1}{\Delta x_j} \int_{I_j} \frac{\partial^m \varphi_{l,i}(x)}{\partial x^m} dx \right) = \delta_m^0 \left(\bar{u}_j - \bar{u}_i \right) + \sum_{l=1}^{k} u_j^l \left(\frac{1}{\Delta x_j} \int_{I_j} \frac{\partial^m \varphi_{l,j}(x)}{\partial x^m} dx \right) \tag{5}$$

where $0 \le m \le M$. We define $\mathbf{u}_i = [u_i^1, u_i^2, ..., u_i^k]^{\mathrm{T}}$ and rewrite Eq. (5) into vector form

$$\mathbf{A}_j^i \mathbf{u}_i = \mathbf{B}_j^i \mathbf{u}_j + \mathbf{b}_j^i \tag{6}$$

where

$$\left(\mathbf{A}_j^i \right)_{ml} = \frac{1}{\Delta x_j} \int_{I_j} \frac{\partial^m \varphi_{l,i}(x)}{\partial x^m} dx, \quad m = 0, ..., M; l = 1, ..., k$$

$$\left(\mathbf{B}_j^i \right)_{ml} = \frac{1}{\Delta x_j} \int_{I_j} \frac{\partial^m \varphi_{l,j}(x)}{\partial x^m} dx, \quad m = 0, ..., M; \; l = 1, ..., k$$

$$\left(\mathbf{b}_j^i \right)_m = \delta_m^0 \left(\bar{u}_j - \bar{u}_i \right), \quad m = 0, ..., M$$

Here S_i is the compact stencil involving only the direct-neighbors or the face-neighbors of I_i. For one-dimensional cases, $S_i = \{ I_{i-1}, I_{i+1} \}$. Therefore, Eq. (6) is equivalent to

$$\mathbf{A}_{i-1}^i \mathbf{u}_i = \mathbf{B}_{i-1}^i \mathbf{u}_{i-1} + \mathbf{b}_{i-1}^i \tag{7}$$

and

$$\mathbf{A}_{i+1}^i \mathbf{u}_i = \mathbf{B}_{i+1}^i \mathbf{u}_{i+1} + \mathbf{b}_{i+1}^i . \tag{8}$$

Since $\mathbf{u}_{i-1}, \mathbf{u}_i$ and $\mathbf{u}_{i+1}$ are all unknown, Eqs. (7)- (8) must be solved implicitly. Furthermore, there are $2(M+1)$ independent relations in Eqs. (7)- (8). In the present paper, we choose $M > k/2 - 1$. As the result, Eqs. (7)- (8) are over-determined and cannot be solved directly. Therefore, the least-squares approach is used to obtain the solvable linear equation system. To be specific, Eqs. (7)- (8) are rearranged into

$$\mathbf{A}_i \mathbf{u}_i = \mathbf{B}_{i-1} \mathbf{u}_{i-1} + \mathbf{B}_{i+1} \mathbf{u}_{i+1} + \mathbf{b}_i \tag{9}$$

where

$$\mathbf{A}_i = \begin{pmatrix} \mathbf{A}_{i-1}^i \\ \mathbf{A}_{i+1}^i \end{pmatrix}, \mathbf{B}_{i-1} = \begin{pmatrix} \mathbf{B}_{i-1}^i \\ \mathbf{0} \end{pmatrix}, \mathbf{B}_{i+1} = \begin{pmatrix} \mathbf{0} \\ \mathbf{B}_{i+1}^i \end{pmatrix}, \mathbf{b}_i = \begin{pmatrix} \mathbf{b}_{i-1}^i \\ \mathbf{b}_{i+1}^i \end{pmatrix}. \tag{10}$$

The following normal equations are obtained using the method of least-squares

$$\left(\mathbf{A}_i^{\mathrm{T}}\mathbf{A}_i\right)\mathbf{u}_i = \left(\mathbf{A}_i^{\mathrm{T}}\mathbf{B}_{i-1}\right)\mathbf{u}_{i-1} + \left(\mathbf{A}_i^{\mathrm{T}}\mathbf{B}_{i+1}\right)\mathbf{u}_{i+1} + \mathbf{A}_i^{\mathrm{T}}\mathbf{b}_i \tag{11}$$

In practice, weight functions $w_{i,m}, m = 0,...,M$ in the form

$$w_{i,m} = \begin{cases} 1, & m = 0 \\ w_m \left(\Delta x_i\right)^m > 0, & m > 0 \end{cases}$$

are introduced and the matrices in Eq. (10) are redefined as

$$\left(\mathbf{A}_j^i\right)_{ml} = \frac{w_{i,m}}{\Delta x_j}\int_{I_j} \frac{\partial^m \varphi_{l,i}(x)}{\partial x^m} dx, \quad m = 0,...,M;\ l = 1,...,k$$

$$\left(\mathbf{B}_j^i\right)_{ml} = \frac{w_{i,m}}{\Delta x_j}\int_{I_j} \frac{\partial^m \varphi_{l,j}(x)}{\partial x^m} dx, \quad m = 0,...,M;\ l = 1,...,k\ .$$

The weight functions are used to control the relative importance of each equation in Eq. (9) and can be also used to fine-tune the spectral properties of the resulting scheme. The determination of w_m will be presented in next subsection. By defining

$$\mathbf{D}_i = \mathbf{A}_i^{\mathrm{T}}\mathbf{A}_i,\ \ \mathbf{E}_i = -\mathbf{A}_i^{\mathrm{T}}\mathbf{B}_{i-1},\ \ \mathbf{F}_i = -\mathbf{A}_i^{\mathrm{T}}\mathbf{B}_{i+1},\ \ \mathbf{g}_i = \mathbf{A}_i^{\mathrm{T}}\mathbf{b}_i$$

Eq. (11) becomes

$$\mathbf{E}_i\mathbf{u}_{i-1} + \mathbf{D}_i\mathbf{u}_i + \mathbf{F}_i\mathbf{u}_{i+1} = \mathbf{g}_i \tag{12}$$

Eq. (12) (i = 2, … , N-1) and additional boundary closures result in a block-tridiagonal system of linear equations which can be solved using the algorithm of Batista [43].

After the introduction of the present reconstruction procedure, several remarks are in order.

***Remark* 1**. The key novelty of the present method is that by the introduction of constitutive relations described in Eq. (4) or Eq. (5), arbitrary order of reconstruction can be performed on a compact stencil. Because this procedure is compact and the reconstruction relation in Eq. (12) is derived using the least-squares method, the reconstruction is called the compact

least-squares (CLS) reconstruction. The FV method that uses the CLS reconstruction will be referenced in what follows as the CLSFV method. The CLS reconstruction is motivated by recent proposals [41,44-46] in designing the accuracy preserving limiters for high order FV and DG schemes. In [41, 44], the SR is proposed which uses the continuations of the reconstruction polynomials on neighboring cells as the additional candidate reconstructions for the current cell. These candidate reconstructions are then used in the WENO [41] and WBAP [44] limiters for the FV schemes. Parallel work designing the WENO limiters for the DG methods is proposed in [45,46]. The success of these limiters suggests a step forward that we can use the continuations of the various order moments of current reconstruction polynomial to match the corresponding moments of the reconstruction polynomials on face-neighboring cells. This is exactly what is being done in the CLS reconstruction.

***Remark* 2**. The present reconstruction scheme is similar to the compact schemes for approximating the derivatives in the finite difference methods in the sense that the reconstruction is performed by solving a system of equations. As a matter of fact, the compact schemes in one-dimensional case do not always use a three-point stencil [47-51]. On the other hand, the combined compact difference (CCD) scheme [52] or the generalized compact scheme [53] uses the constitutive relation of high order spatial derivatives to maintain a three-point stencil, which is therefore closer to the present method. Of course, the design of the present method is based on the integral relations, which is fundamentally different with the compact finite difference schemes mentioned above. Furthermore, the present method is intended to be implemented on the unstructured grids while other compact finite volume

schemes [54-57] are all based on the structured grids.

***Remark* 3**. In the present paper, we choose $M = k$-1. In this case, the number of equations in Eq. (9) doubles the unknowns, and Eq. (12) is therefore a validated relation to perform arbitrary order of reconstruction on the compact stencil $S_i = \{I_{i-1}, I_{i+1}\}$. The physical motivation of the introduction of the weight functions in the least square procedure is to the spectral properties of the resulting schemes. The free parameters w_m involved in the weight functions can be adjusted to achieve optimal spectral properties, which provides a natural way to determine the optimal values of these free parameters. Additional details will be given in next subsection.

***Remark* 4**. The boundary closure procedure of the CLS reconstruction is straightforward. For a boundary cell, there is only one face neighboring cell. If $M = k$-1 is chosen, the number of equations in Eq. (9) equals the number of unknowns. Therefore, Eq. (12) is still a validated relation to perform arbitrary order of reconstruction by simply removing the $\mathbf{E}_i\mathbf{u}_{i-1}$ term at the left boundary or the $\mathbf{F}_i\mathbf{u}_{i+1}$ term at the right boundary. This is sufficient to handle the far-field and reflective boundary conditions. Taking the left boundary as an example, the right state at the left interface of the boundary cell is computed directly using the reconstruction polynomial, and the left state is provided by the boundary condition. Then a Riemann solver is applied to compute the boundary numerical flux. One can also choose $M = k$ for which the number of equations in Eq. (9) is larger than the number of unknowns. In this case, the Dirichlet boundary condition can be accommodated by using the constrained CLS

reconstruction.

***Remark* 5**. The present reconstruction procedure will be generalized to multi-dimensional cases in a future paper. There is no efficient direct solver to solve the counterpart of Eq. (12) in multi-dimensional cases. Therefore, it will be solved using an iteration method. One may wonder the efficiency of the present reconstruction scheme when it is solved using the iteration method. The forthcoming paper will show that, in several important situations, the present method is as efficient as the traditional *k*-exact reconstruction in terms the absolute computational cost while in terms of CPU time for achieving the same accuracy, the present method can be much more efficient.

Before concluding this subsection, the formulations of Eq. (9) when performing the linear to quintic polynomial reconstructions are presented. The uniform meshes are assumed for simplicity.

The linear reconstruction.

$$\begin{aligned} &\mathbf{A}_i = \begin{bmatrix} -1 \\ 1 \end{bmatrix}, \mathbf{B}_{i-1} = \mathbf{0}, \mathbf{B}_{i+1} = \mathbf{0}, \\ &\mathbf{u}_i = u_i^1, \mathbf{b}_i = \begin{pmatrix} \overline{u}_{i-1} - \overline{u}_i \\ \overline{u}_{i+1} - \overline{u}_i \end{pmatrix}. \end{aligned} \tag{13}$$

The quadratic reconstruction.

$$\mathbf{A}_i = \begin{bmatrix} -1 & 1 \\ w_1 & -2w_1 \\ 1 & 1 \\ w_1 & 2w_1 \end{bmatrix}, \mathbf{B}_{i-1} = \begin{bmatrix} 0 & 0 \\ w_1 & 0 \\ 0 & 0 \\ 0 & 0 \end{bmatrix}, \mathbf{B}_{i+1} = \begin{bmatrix} 0 & 0 \\ 0 & 0 \\ 0 & 0 \\ w_1 & 0 \end{bmatrix},$$
$$\mathbf{u}_i = \begin{pmatrix} u_i^1 \\ u_i^2 \end{pmatrix}, \mathbf{b}_i = \begin{pmatrix} \bar{u}_{i-1} - \bar{u}_i \\ 0 \\ \bar{u}_{i+1} - \bar{u}_i \\ 0 \end{pmatrix}. \tag{14}$$

The cubic reconstruction.

$$\mathbf{A}_i = \begin{bmatrix} -1 & 1 & -5/4 \\ w_1 & -2w_1 & 13w_1/4 \\ 0 & 2w_2 & -6w_2 \\ 1 & 1 & 5/4 \\ w_1 & 2w_1 & 13w_1/4 \\ 0 & 2w_2 & 6w_2 \end{bmatrix}, \mathbf{B}_{i-1} = \begin{bmatrix} 0 & 0 & 0 \\ w_1 & 0 & w_1/4 \\ 0 & 2w_2 & 0 \\ 0 & 0 & 0 \\ 0 & 0 & 0 \\ 0 & 0 & 0 \end{bmatrix},$$
$$\mathbf{B}_{i+1} = \begin{bmatrix} 0 & 0 & 0 \\ 0 & 0 & 0 \\ 0 & 0 & 0 \\ 0 & 0 & 0 \\ w_1 & 0 & w_1/4 \\ 0 & 2w_2 & 0 \end{bmatrix}, \mathbf{u}_i = \begin{pmatrix} u_i^1 \\ u_i^2 \\ u_i^3 \end{pmatrix}, \mathbf{b}_i = \begin{pmatrix} \bar{u}_{i-1} - \bar{u}_i \\ 0 \\ 0 \\ \bar{u}_{i+1} - \bar{u}_i \\ 0 \\ 0 \end{pmatrix}. \tag{15}$$

The quartic reconstruction.

$$\mathbf{A}_i = \begin{bmatrix} -1 & 1 & -5/4 & 3/2 \\ w_1 & -2w_1 & 13w_1/4 & -5w_1 \\ 0 & 2w_2 & -6w_2 & 13w_2 \\ 0 & 0 & 6w_3 & -24w_3 \\ 1 & 1 & 5/4 & 3/2 \\ w_1 & 2w_1 & 13w_1/4 & 5w_1 \\ 0 & 2w_2 & 6w_2 & 13w_2 \\ 0 & 0 & 6w_3 & 24w_3 \end{bmatrix}, \mathbf{B}_{i-1} = \begin{bmatrix} 0 & 0 & 0 & 0 \\ w_1 & 0 & w_1/4 & 0 \\ 0 & 2w_2 & 0 & w_2 \\ 0 & 0 & 6w_3 & 0 \\ 0 & 0 & 0 & 0 \\ 0 & 0 & 0 & 0 \\ 0 & 0 & 0 & 0 \\ 0 & 0 & 0 & 0 \end{bmatrix},$$

$$\mathbf{B}_{i+1}=\begin{bmatrix}0&0&0&0\\0&0&0&0\\0&0&0&0\\0&0&0&0\\0&0&0&0\\w_1&0&w_1/4&0\\0&2w_2&0&w_2\\0&0&6w_3&0\end{bmatrix},\mathbf{u}_i=\begin{pmatrix}u_i^1\\u_i^2\\u_i^3\\u_i^4\end{pmatrix},\mathbf{b}_i=\begin{pmatrix}\bar{u}_{i-1}-\bar{u}_i\\0\\0\\0\\\bar{u}_{i+1}-\bar{u}_i\\0\\0\\0\end{pmatrix}. \qquad (16)$$

The quintic reconstruction.

$$\mathbf{A}_i=\begin{bmatrix}-1&1&-5/4&3/2&-91/48\\w_1&-2w_1&13w_1/4&-5w_1&121w_1/16\\0&2w_2&-6w_2&13w_2&-25w_2\\0&0&6w_3&-24w_3&65w_3\\0&0&0&24w_4&-120w_4\\1&1&5/4&3/2&91/48\\w_1&2w_1&13w_1/4&5w_1&121w_1/16\\0&2w_2&6w_2&13w_2&25w_2\\0&0&6w_3&24w_3&65w_3\\0&0&0&24w_4&120w_4\end{bmatrix},\mathbf{B}_{i-1}=\begin{bmatrix}0&0&0&0&0\\w_1&0&w_1/4&0&w_1/16\\0&2w_2&0&w_2&0\\0&0&6w_3&0&5w_3\\0&0&0&24w_4&0\\0&0&0&0&0\\0&0&0&0&0\\0&0&0&0&0\\0&0&0&0&0\\0&0&0&0&0\end{bmatrix},$$

$$\mathbf{B}_{i+1}=\begin{bmatrix}0&0&0&0&0\\0&0&0&0&0\\0&0&0&0&0\\0&0&0&0&0\\0&0&0&0&0\\0&0&0&0&0\\w_1&0&w_1/4&0&w_1/16\\0&2w_2&0&w_2&0\\0&0&6w_3&0&5w_3\\0&0&0&24w_4&0\end{bmatrix},\mathbf{u}_i=\begin{pmatrix}u_i^1\\u_i^2\\u_i^3\\u_i^4\\u_i^5\end{pmatrix},\mathbf{b}_i=\begin{pmatrix}\bar{u}_{i-1}-\bar{u}_i\\0\\0\\0\\0\\\bar{u}_{i+1}-\bar{u}_i\\0\\0\\0\\0\end{pmatrix}. \qquad (17)$$

For the linear reconstruction, the present approach is identical to the linear *k*-exact reconstruction and no linear equation system needs to be solved. The reconstructed slope is

$$u_i^1 = \frac{\bar{u}_{i+1} - \bar{u}_{i-1}}{2}.$$

For higher order reconstructions, linear equation systems similar to the compact finite difference schemes are solved to determine the coefficients in the reconstruction polynomials.

It is shown in Eqs. (13)- (17) that the reconstruction matrix is invariant with respect to grid scaling, due to the use of the normalized zero-mean basis in Eq. (2). The condition number of the matrix $\mathbf{A}_i$ of the linear reconstruction is 1, while the condition number of the high order reconstruction depends on the free parameters w_m. With the optimal values of the free parameters obtained in next subsection, the condition number of the quadratic reconstruction ($w_1 = 0$) is 1 and the condition number of the cubic reconstruction $(w_1 = 0.01, w_2 = 0.01)$ is 40.57. It should be pointed out that the free parameters are optimized to produce the best spectral properties rather than the smallest condition number, thus the optimal parameters do not result in the minimal condition number. Numerical experiments indicate that the reconstruction procedures do not experience convergence difficulty in the practical computations.

2.2 Fourier analysis

In this subsection, the CLSFV scheme of the one-dimensional scalar linear advection equation will be presented and the dispersion/dissipation and stability properties of CLSFV will be studied. The governing equation is

$$\frac{\partial u}{\partial t}+\frac{\partial f}{\partial x}=0 \tag{18}$$

where the flux is $f = au$ and a is a constant. For simplicity, assume that a is positive and the grids are uniform, i.e., $a > 0$ and $\Delta x_i = h$. The integral form of Eq. (18) on control volume I_i is

$$\frac{\partial \overline{u}_i}{\partial t}=-\frac{1}{h}\left(f_{i+1/2}-f_{i-1/2}\right) \tag{19}$$

where $f_{i\pm1/2}=au\left(x_{i\pm1/2}\right)$ are the exact fluxes.

The semi-discrete finite volume scheme approximates Eq. (17) by the introduction of numerical fluxes $\hat{f}_{i\pm1/2}$ so that

$$\frac{\partial \overline{u}_i}{\partial t}=-\frac{1}{h}\left(\hat{f}_{i+1/2}-\hat{f}_{i-1/2}\right).$$

When upwind fluxes are used, the numerical flux is

$$\hat{f}_{i+1/2}=\hat{f}\left(u^L_{i+1/2},u^R_{i+1/2}\right)=au^L_{i+1/2} \tag{20}$$

for $a > 0$, where $u^L_{i+1/2}$ and $u^R_{i+1/2}$ are calculated by the reconstruction polynomials on I_i and I_{i+1},

$$\begin{aligned} u^L_{i+1/2}&=u_i(x_{i+1/2})=\overline{u}_i+\sum_{l=1}^{k}u^l_i\varphi_{l,i}(x_{i+1/2}),\\ u^R_{i+1/2}&=u_{i+1}(x_{i+1/2})=\overline{u}_{i+1}+\sum_{l=1}^{k}u^l_{i+1}\varphi_{l,i+1}(x_{i+1/2}). \end{aligned} \tag{21}$$

The coefficients u^l_i and u^l_{i+1} in Eq. (21) are determined by the reconstruction procedure presented in Section 2.1.

Next, a Fourier analysis is performed to study the spectral behavior of the second, third and fourth order CLSFV schemes. It is understood that the corresponding CLS reconstructions are linear, quadratic and cubic. The solution is considered to be a single Fourier

mode $u(x,t) = A_m(t)e^{ik_m x}$. Its cell average is

$$\bar{u}_i = \frac{A_m}{\mathrm{i}\,k_m h}\left(e^{\mathrm{i}k_m x_{i+1/2}} - e^{\mathrm{i}k_m x_{i-1/2}}\right). \tag{22}$$

The exact fluxes in Eq. (19) are

$$f_{i\pm1/2} = aA_m e^{\mathrm{i}k_m x_{i\pm1/2}}. \tag{23}$$

Therefore, in Fourier space, the exact integral equation becomes

$$\frac{\partial A_m}{\partial t} + \mathrm{i}\,k_m a A_m = 0.$$

Similarly, the semi-discrete finite volume scheme in Fourier space can be written as

$$\frac{\partial A_m}{\partial t} + \mathrm{i}\,k'_m a A_m = 0 \tag{24}$$

with

$$\frac{k'_m}{k_m} = \frac{\hat{f}_{i+1/2} - \hat{f}_{i-1/2}}{f_{i+1/2} - f_{i-1/2}}.$$

$\hat{f}_{i\pm1/2}$ are computed in Fourier space using Eq. (20) where the interfacial values $u^{L,R}_{i+1/2}$ are determined using Eq. (21) with the coefficients obtained through the reconstruction in terms of the cell-averages defined in Eq. (22). It is convenient to introduce a scaled wavenumber $\kappa = k_m h \in (0,\pi]$ so that $\kappa' = k'_m h$ is expressed by

$$\kappa' = \frac{\hat{f}_{i+1/2} - \hat{f}_{i-1/2}}{f_{i+1/2} - f_{i-1/2}}\kappa.$$

κ' is called the modified wavenumber whose real part $\mathrm{Re}(\kappa')$ and the imaginary part $\mathrm{Im}(\kappa')$ are associated respectively with the dispersion and dissipation properties of the FV scheme. The expressions of the modified wavenumbers of the second, third and fourth order CLSFV schemes are given below.

The second order CLSFV scheme.

$$\begin{aligned}\mathrm{Re}(\kappa') &= \frac{3}{2}\sin(\kappa)-\frac{1}{4}\sin(2\kappa)\\ \mathrm{Im}(\kappa') &= -\frac{3}{4}+\cos(\kappa)-\frac{1}{4}\cos(2\kappa).\end{aligned} \tag{25}$$

The third order CLSFV scheme.

$$\begin{aligned}\mathrm{Re}(\kappa') &= \frac{\left[16+79w_1^{\,2}+48w_1^{\,4}-4\left(1+8w_1^{\,2}+12w_1^{\,4}\right)\cos(\kappa)+w_1^{\,2}\cos(2\kappa)\right]\sin(\kappa)}{12\left(1+4w_1^{\,2}\right)\left(1+w_1^{\,2}-w_1^{\,2}\cos(\kappa)\right)}\\ \mathrm{Im}(\kappa') &= -\frac{2\left[2+15w_1^{\,2}+24w_1^{\,4}-w_1^{\,2}\cos(\kappa)\right]\sin^4(\kappa/2)}{3\left(1+4w_1^{\,2}\right)\left(1+w_1^{\,2}-w_1^{\,2}\cos(\kappa)\right)}.\end{aligned} \tag{26}$$

The fourth order CLSFV scheme.

$$\begin{aligned}\mathrm{Re}(\kappa') &= \frac{s_1*\sin(\kappa)+s_2*\sin(2\kappa)+s_3*\sin(3\kappa)}{c_0+c_1*\cos(\kappa)+c_2*\cos(2\kappa)}\\ \mathrm{Im}(\kappa') &= \frac{-s_4*\sin^6(\kappa/2)}{c_3+c_4*\cos(\kappa)+c_5*\cos(2\kappa)}\end{aligned} \tag{27}$$

where

$$\begin{cases} s_1 = w_1^{\,2}\left(77+318w_1^{\,2}\right)+6\left(111+538w_1^{\,2}+180w_1^{\,4}\right)w_2^{\,2}+216\left(13+10w_1^{\,2}\right)w_2^{\,4}\\ s_2 = -4\left[w_1^{\,2}+6w_1^{\,4}+6\left(6+41w_1^{\,2}+36w_1^{\,4}\right)w_2^{\,2}+432\left(1+w_1^{\,2}\right)w_2^{\,4}\right]\\ s_3 = \left(1+6w_1^{\,2}+12w_2^{\,2}\right)\left[w_1^{\,2}+18\left(1+2w_1^{\,2}\right)w_2^{\,2}\right]\\ s_4 = 4\left(1+6w_1^{\,2}+12w_2^{\,2}\right)\left[w_1^{\,2}+18\left(1+2w_1^{\,2}\right)w_2^{\,2}\right]\end{cases} \tag{28}$$

and

$$\begin{cases} c_0 = 48\left(w_1^{\,2}+4w_1^{\,4}\right)+432\left(1+5w_1^{\,2}+3w_1^{\,4}\right)w_2^{\,2}+864\left(2+3w_1^{\,2}\right)w_2^{\,4}\\ c_1 = -24\left[72w_2^{\,4}+w_1^{\,4}\left(-4+72w_2^{\,2}\right)+w_1^{\,2}\left(-1+22w_2^{\,2}+144w_2^{\,4}\right)\right]\\ c_2 = 48w_1^{\,2}w_2^{\,2}(2+9w_1^{\,2}+18w_2^{\,2})\\ c_3 = 6w_1^{\,2}+24w_1^{\,4}+54\left(1+5w_1^{\,2}+3w_1^{\,4}\right)w_2^{\,2}+108\left(2+3w_1^{\,2}\right)w_2^{\,4}\\ c_4 = -216w_2^{\,4}-3w_1^{\,4}\left(-4+72w_2^{\,2}\right)-3w_1^{\,2}\left(-1+22w_2^{\,2}+144w_2^{\,4}\right)\\ c_5 = 6w_1^{\,2}w_2^{\,2}(2+9w_1^{\,2}+18w_2^{\,2}).\end{cases} \tag{29}$$

According to Eqs. (25)- (29), there is one free parameter w_1 in the third order scheme and

two free parameters (w_1, w_2) in the fourth order scheme. To give specific values of these free parameters for practical use, an optimization procedure is performed by minimizing the following cost function [58]

$$E = \frac{1}{e^{\nu\pi}} \int_0^{\pi} e^{\nu(\pi-\kappa)} \left(\mathrm{Re}(\kappa') - \kappa\right)^2 d\kappa . \tag{30}$$

The parameter *v* in Eq. (30) is used to control the relative importance of the low wavenumber and high wavenumber errors. A larger *v* will emphasis more the contribution of the low wavenumber error. For the third order scheme, the optimal value of the only free parameter is $w_1 = 0$ regardless of the value of *v*; for the fourth order scheme, the optimal values of (w_1, w_2) corresponding to different values of *v* are listed in Table 1. Two pairs of free parameters are chosen for practical applications, namely $(w_1 = 0.01, w_2 = 0.01)$ which is corresponding to $v = 80$ in Table 1, and $(w_1 = 1, w_2 = 0)$ which is corresponding to $v = 4$ in Table 1.

Table 1. Optimized values of (w_1 , w_2) due to different *v*.

v	2	4	6	8	10	20	40	60	80
w_1	$>10^4$	1	$<10^{-4}$	0.0200	0.0100	0.0100	0.0100	0.0100	0.0100
w_2	0	0	0	0.0360	0.0490	0.0196	0.0144	0.0121	0.0100

The dispersion and dissipation properties of the second, third and fourth order CLSFV schemes are shown in Fig. 2. The spectral properties of the sixth order central difference scheme (C6) and the sixth order tridiagonal scheme (T6) proposed in [47] are also shown in Fig. 2 for the purpose of comparison. Specifically, for the third order and fourth order CLSFV schemes, the dispersion and dissipation properties are corresponding to the optimal

parameters presented above. For the fourth order scheme, the parameters $(w_1 = 0.01, w_2 = 0.01)$ result in smaller dispersion error for low wavenumber components, while the parameters $(w_1 = 1, w_2 = 0)$ result in larger bandwidth in which higher wavenumber components can be captured with relatively small dispersion error. To show this more clearly, the relative dispersion error defined by $\mathrm{Re}(\kappa')/\kappa - 1$ is plotted in Fig. 3. For $(w_1 = 0.01, w_2 = 0.01)$, the bandwidth with relative phase error $\left|\mathrm{Re}(\kappa')/\kappa - 1\right| \le 0.5\%$ is $\kappa \in (0, 1.23]$ and the bandwidth with relative phase error $\left|\mathrm{Re}(\kappa')/\kappa - 1\right| \le 3\%$ is $\kappa \in (0, 1.51]$. For $(w_1 = 1, w_2 = 0)$, the bandwidth with relative phase error $\left|\mathrm{Re}(\kappa')/\kappa - 1\right| \le 0.5\%$ is $\kappa \in (0, 0.82]$ and the bandwidth with relative phase error $\left|\mathrm{Re}(\kappa')/\kappa - 1\right| \le 3\%$ is $\kappa \in (0, 2.10]$. In both cases, the fourth order scheme produces the resolving bandwidth considerably larger than that of the second and third order schemes for the same tolerance of phase errors. The dispersion of the present fourth order scheme lies in between the C6 and T6 for $(w_1 = 0.01, w_2 = 0.01)$. And for $(w_1 = 1, w_2 = 0)$, the present fourth order scheme achieves larger resolving bandwidth than both C6 and T6 under the tolerance $\left|\mathrm{Re}(\kappa')/\kappa - 1\right| \le 3\%$ at the expense of larger phase error at lower wavenumbers. It should be pointed out that the C6 and T6 schemes are not dissipative, and a certain filtering procedure is needed to maintain stability. On the other hand, the present schemes are dissipative because of the use of upwind technique in computing the numerical flux. In practice, no filtering technique is required.

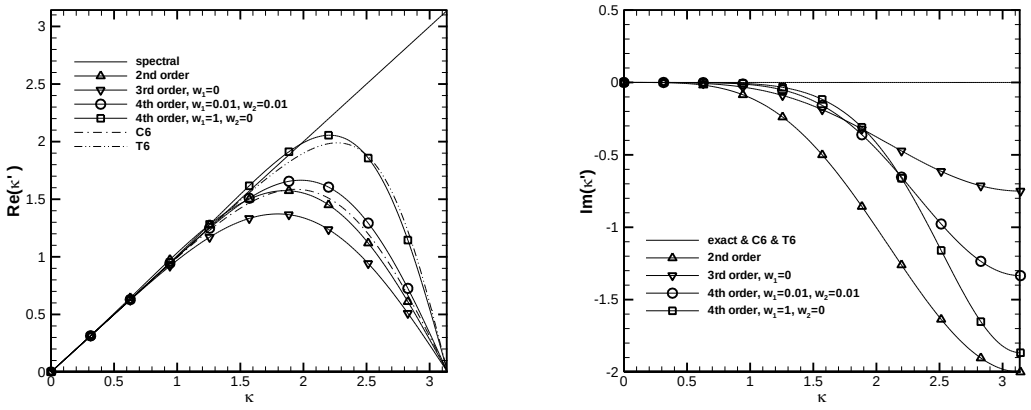

Fig. 2. Dispersion and dissipation properties of the second to fourth order CLSFV schemes.

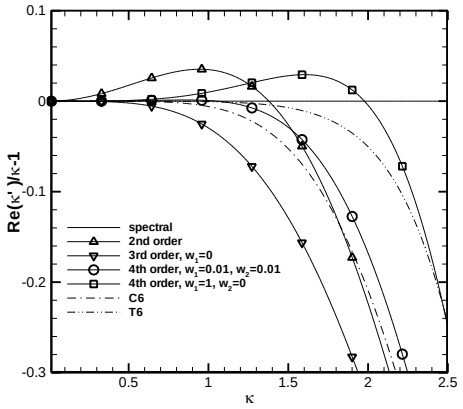

Fig. 3. Dispersion errors of the second to fourth order CLSFV schemes.

In what follows, the von-Neumann stability analysis of the present FV schemes will be presented. Equation (24) is rewritten as

$$\frac{\partial A_m}{\partial t} = -\frac{\mathrm{i}\kappa' c}{\Delta t} A_m . \tag{31}$$

where $c = a\Delta t / h$ is the Courant or CFL number. Equation (31) is temporally discretized using the three stage TVD Runge-Kutta scheme [32]. The amplification factor can be derived as

$$G_m = \frac{A_m^{n+1}}{A_m^n} = 1/3 + \left(1+Z\right)/2 + \left(1+Z\right)^3/6$$

where $Z=-\mathrm{i}c\kappa'$. The scheme is stable if $|G_m|\le 1$ for all $\kappa\in(0,\pi]$. For high order FV method, it is difficult to derive the analytical stability condition because of the complexity of Z or κ'. Therefore, the stability is analyzed numerically. Specifically, the relations between $|G_m|$ and $\kappa\in(0,\pi]$ for various Courant numbers are depicted in Fig. 4 for the present FV schemes. According to Fig. 4, for $\kappa\in(0,\pi]$, the proposed FV schemes are stable if $c\le 1.1$. However, when $c\ge 1.2$, the second order scheme and the fourth order scheme with $(w_1=1,w_2=0)$ become unstable since there are certain wavenumbers for which $|G_m|>1$. Therefore, there is a critical Courant number $c_{crit}\in(1.1,1.2)$ below which all schemes are stable. Figure 4 also shows that the fourth order scheme with $(w_1=0.01,w_2=0.01)$ is better than that with $(w_1=1,w_2=0)$ in terms of the stability property. In the remainder of this paper, unless otherwise indicated, the third order scheme uses the parameter $w_1=0$ and the fourth order scheme uses the parameters $(w_1=0.01,w_2=0.01)$.

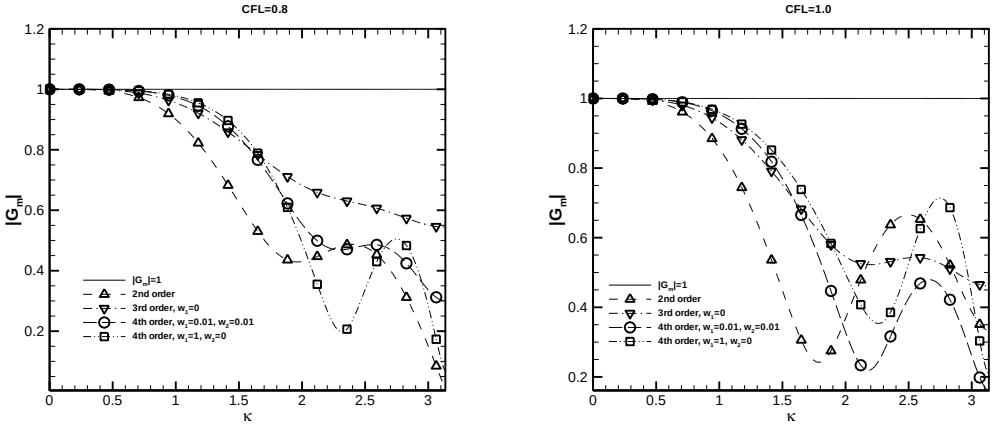

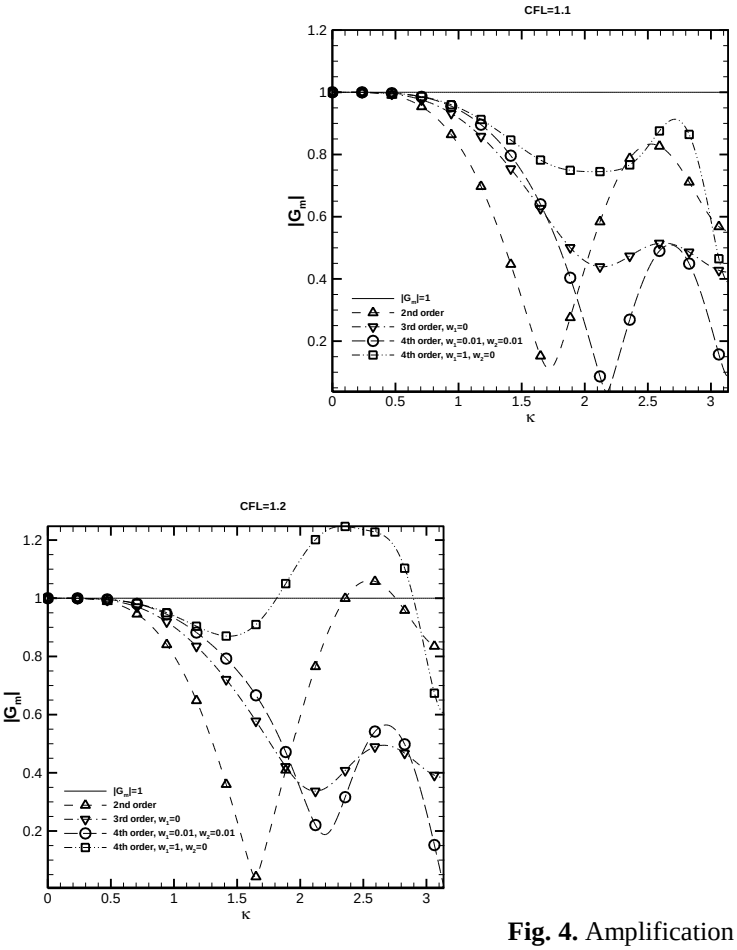

Fig. 4. Amplification factors for the CLSFV schemes using TVD RK3. The CFL numbers are 0.8, 1.0, 1.1, and 1.2.

3 High order CLSFV schemes for 1D Euler equations

In this section, the CLSFV method is used to solve the one-dimensional non-linear Euler equations, which in conversation form can be written as

$$\frac{\partial \mathbf{U}}{\partial t}+\frac{\partial \mathbf{F}}{\partial x}=0 \tag{32}$$

where $\mathbf{U}$ is vector of the conservative variables and $\mathbf{F}$ is the flux vector defined respectively by

$$\mathbf{U}=\left(\rho,\ \rho u,\ \rho E\right)^{\mathrm{T}},\ \mathbf{F}=\left(\rho u,\ \rho u^{2}+p, u\left(\rho E+p\right)\right)^{\mathrm{T}}.$$

The semi-discrete FV scheme of Eq. (32) on control volume I_i is

$$\frac{\partial \overline{\mathbf{U}}_i}{\partial t} = -\frac{1}{\Delta x_i}\left(\hat{\mathbf{F}}_{i+1/2} - \hat{\mathbf{F}}_{i-1/2}\right). \tag{33}$$

Given the mesh partition with the control volumes defined by $I_i \equiv \left[x_{i-1/2}, x_{i+1/2}\right]$, $i = 1, \cdots, N$, the procedure to implement the FV scheme consists of the following steps.

1). The CLS reconstruction is applied to each component of the conservative variables to obtain the reconstruction polynomial

$$\mathbf{U}_i(x) = \bar{\mathbf{U}}_i + \sum_{l=1}^{k} \mathbf{U}_i^l \varphi_{l,i}(x) . \tag{34}$$

2). If there are discontinuities in the solution, a limiting procedure is applied to Eq. (34) to modify the coefficients $\mathbf{U}_i^l$ into $\tilde{\mathbf{U}}_i^l$ to suppress the possible oscillations in the vicinity of the flow discontinuities. In the present paper, the WBAP limiter [44, 59] is used. The detailed formulations of the WBAP limiter will be presented later in the present section.

3). The left and right states $\mathbf{U}_{i+1/2}^L$ and $\mathbf{U}_{i+1/2}^R$ at the cell interface $x = x_{i+1/2}$ are calculated using the reconstruction polynomials on I_i and I_{i+1} with

$$\mathbf{U}_{i+1/2}^L = \mathbf{U}_i(x_{i+1/2}) = \bar{\mathbf{U}}_i + \sum_{l=1}^{k} \tilde{\mathbf{U}}_i^l \varphi_{l,i}(x_{i+1/2}),$$
$$\mathbf{U}_{i+1/2}^R = \mathbf{U}_{i+1}(x_{i+1/2}) = \bar{\mathbf{U}}_{i+1} + \sum_{l=1}^{k} \tilde{\mathbf{U}}_{i+1}^l \varphi_{l,i+1}(x_{i+1/2}).$$

4). The numerical flux $\hat{\mathbf{F}}_{i+1/2} = \hat{\mathbf{F}}\left(\mathbf{U}_{i+1/2}^L, \mathbf{U}_{i+1/2}^R\right)$ is evaluated by a specified Riemann solver. This paper uses a modified Roe Riemann solver which is the standard Roe Riemann solver [60] using the Lax-Friedrich flux as the entropy fix. Specifically, the absolute value of each eigenvalue appeared in the formulation of Roe's Riemann solver is modified as:

$$\left|\tilde{\lambda}_l\right| = \begin{cases} \max\left(\left|\lambda_m\right|\right), & \textit{if } \exists \left|\lambda_m\right| < \beta c,\ m = 1,2,3 \\ \left|\lambda_l\right|, & \textit{otherwise} \end{cases}$$

where c is the speed of sound and β is a free parameter chosen usually between 0.05 and 0.15.

5). After computing the numerical flux, Eq. (33) is temporally integrated by means of the three-stage TVD Runge-Kutta scheme.

In what follows, the limiting procedure for computing $\tilde{\mathbf{U}}_i^l$ will be presented. The limiting procedure is basically the WBAP limiter proposed in [44] for high order FV schemes. The reconstruction polynomial described in Eq. (34), which is called the primary reconstruction polynomial in the present paper, is obtained on every control volume by the CLS reconstruction. To apply the WBAP limiter on $I_i \equiv \left[x_{i-1/2}, x_{i+1/2}\right]$, besides $\mathbf{U}_i(x)$, two additional reconstruction polynomials approximating $\mathbf{U}(x)$ on I_i to the same order of accuracy as $\mathbf{U}_i(x)$ need to be provided. In the WBAP limiter, this is achieved by the so called secondary reconstruction (SR) technique [41,44] which uses the continuations of the primary reconstructions on $I_j \in S_i = \{I_{i-1}, I_{i+1}\}$ as the additional candidate reconstructions. Specifically, the secondary reconstruction in terms of $\mathbf{U}_j(x)$ is

$$\mathbf{U}_{j\to i}(x) = \bar{\mathbf{U}}_i + \sum_{l=1}^{k} \mathbf{U}_{j\to i}^l \varphi_{l,i}(x)$$

where

$$\mathbf{U}_{j\to i}^l = \frac{1}{l!}\frac{\partial^l \mathbf{U}_j(x)}{\partial x^l}\bigg|_{x=x_i} \cdot (\Delta x_i)^l .$$

For the cubic reconstruction, we have

$$\begin{aligned}
\mathbf{U}^1_{j\to i} &= \left[\mathbf{U}^1_j + 2\mathbf{U}^2_j \delta x_j + 3\mathbf{U}^3_j \left(\delta x_j\right)^2\right]\cdot\left(\Delta x_i / \Delta x_j\right) \\
\mathbf{U}^2_{j\to i} &= \left(\mathbf{U}^2_j + 3\mathbf{U}^3_j \delta x_j\right)\cdot\left(\Delta x_i / \Delta x_j\right)^2 \\
\mathbf{U}^3_{j\to i} &= \mathbf{U}^3_j \cdot\left(\Delta x_i / \Delta x_j\right)^3
\end{aligned} \tag{35}$$

where $\delta x_j = \left(x_i - x_j\right)/\Delta x_j$. After performing the secondary reconstructions on $I_j \in S_i = \left\{I_{i-1}, I_{i+1}\right\}$, three reconstruction polynomials with the same order of accuracy on I_i are obtained, namely the primary reconstruction $\mathbf{U}_i(x)$ and two secondary reconstructions $\mathbf{U}_{i-1\to i}(x)$ and $\mathbf{U}_{i+1\to i}(x)$.

In the WBAP limiter, the limited coefficient $\tilde{\mathbf{U}}^l_i$ is computed by a non-linear average of $\mathbf{U}^l_i$, $\mathbf{U}^l_{i-1\to i}$ and $\mathbf{U}^l_{i+1\to i}$ in the form

$$\tilde{\mathbf{U}}^l_i = L(\mathbf{U}^l_i, \mathbf{U}^l_{i-1\to i}, \mathbf{U}^l_{i+1\to i})$$

where

$$L(a_0, a_1, a_2, \ldots, a_J) = a_0 \cdot W(1, \frac{a_1}{a_0}, \frac{a_2}{a_0}, \ldots, \frac{a_J}{a_0}) .$$

W is the WBAP operator which is functionally identical to the limiters in the shock capturing schemes such as the TVD schemes [61, 62]. There are several possible choices of *W*. In the present paper, the WBAP-L2 limiter [59]

$$W = W^{L2}(1, \theta_1, \cdots, \theta_J) = \frac{n_P + \sum_{k=1}^{J} 1/\theta_k^{p-1}}{n_P + \sum_{k=1}^{J} 1/\theta_k^{p}} \tag{36}$$

is used. In this paper, *p* is chosen as *p* = 4 , and n_P = 10 is used to emphasize the contribution of the first argument of *W* corresponding to the coefficient of the primary reconstruction.

The underlying theory behind the WBAP limiter can be found in [44, 59] and is thus

omitted here. It is observed that when applying the technique presented above to the FV schemes higher than second order, it is not sufficient to remove the oscillations in the vicinity of shock waves. To solve this problem, the successive limiting procedure [44] is used. Furthermore, the limiter in terms of the characteristic variables can obtain better results in terms of robustness and shock capturing capability [44]. In the present paper, an improved successive limiting procedure in terms of the characteristic variables is proposed which is similar to the technique used in [46] for WENO limiter of the DG schemes. The remainder of this section will present the application of this procedure to the fourth order FV scheme. Applications to other schemes are straightforward.

The cell interface between I_i and $I_j \in S_i = \{I_{i-1}, I_{i+1}\}$ is denoted with $m = (i+j)/2$. The improved successive limiting procedure in terms of the characteristic variables consists of the following steps.

1) The characteristic variables corresponding to the third order derivatives of the primary and secondary reconstructions, namely $\mathbf{U}_i^3$ and $\mathbf{U}_{j\to i}^3 = \mathbf{U}_j^3 \cdot \left(\Delta x_i / \Delta x_j\right)^3$ are computed by

$$\mathbf{V}_i^{3,m} = (\mathbf{R}^m)^{-1}\mathbf{U}_i^3$$
$$\mathbf{V}_{j\to i}^{3,m} = (\mathbf{R}^m)^{-1}\mathbf{U}_{j\to i}^3$$

where $\mathbf{R}^m$ is the matrix of the right eigenvectors of the Jacobian matrix of Euler equations associated with the interface m. The WBAP limiter is applied to each component of $\mathbf{V}_i^{3,m}$ and $\mathbf{V}_{j\to i}^{3,m}$ using

$$\tilde{\mathbf{V}}_i^{3,m} = L(\mathbf{V}_i^{3,m}, \mathbf{V}_{j\to i}^{3,m}).$$

This procedure is executed twice for $j = i-1$ and $j = i+1$, namely $m = i-1/2$ and $i+1/2$. After computing $\tilde{\mathbf{V}}_i^{3,i\pm1/2}$, the corresponding $\tilde{\mathbf{U}}_i^{3,i\pm1/2}$ are deduced using

$$\tilde{\mathbf{U}}_i^{3,i\pm1/2} = \mathbf{R}^{i\pm1/2}\tilde{\mathbf{V}}_i^{3,i\pm1/2}$$

Finally, the limited $\tilde{\mathbf{U}}_i^3$ is computed using

$$\tilde{\mathbf{U}}_i^3 = L(\tilde{\mathbf{U}}_i^{3,i-1/2}, \tilde{\mathbf{U}}_i^{3,i+1/2})$$

in which the parameter $n_P = 1$ as every interface is treated equally.

2) For $I_j \in S_i = \{I_{i-1}, I_{i+1}\}$, the second order derivatives of the secondary reconstructions are computed by

$$\mathbf{U}_{j\to i}^2 = \left(\mathbf{U}_j^2 + 3\tilde{\mathbf{U}}_j^3 \delta x_j\right) \cdot \left(\Delta x_i / \Delta x_j\right)^2 .$$

It should be noted that in the successive limiting procedure, the third order derivative used to compute $\mathbf{U}_{j\to i}^2$ is the limited $\tilde{\mathbf{U}}_j^3$. Then the second order derivatives of the primary and secondary reconstructions are projected to the characteristic space using

$$\begin{aligned} \mathbf{V}_i^{2,m} &= (\mathbf{R}^m)^{-1}\mathbf{U}_i^2 \\ \mathbf{V}_{j\to i}^{2,m} &= (\mathbf{R}^m)^{-1}\mathbf{U}_{j\to i}^2 \end{aligned} .$$

The procedure in 1) is repeated to compute the limited $\tilde{\mathbf{U}}_i^2$.

3) For $I_j \in S_i = \{I_{i-1}, I_{i+1}\}$, the first order derivatives of the secondary reconstructions are computed by

$$\mathbf{U}_{j\to i}^1 = \left[\mathbf{U}_j^1 + 2\tilde{\mathbf{U}}_j^2 \delta x_j + 3\tilde{\mathbf{U}}_j^3 \left(\delta x_j\right)^2\right] \cdot \left(\Delta x_i / \Delta x_j\right) .$$

Then the first order derivatives of the primary and secondary reconstructions are projected to the characteristic space using

$$\begin{aligned} \mathbf{V}_i^{1,m} &= (\mathbf{R}^m)^{-1}\mathbf{U}_i^1 \\ \mathbf{V}_{j\to i}^{1,m} &= (\mathbf{R}^m)^{-1}\mathbf{U}_{j\to i}^1 \end{aligned} .$$

The procedure of 1) or 2) is repeated to compute the limited $\tilde{\mathbf{U}}_i^1$.

Since the present limiting procedure in characteristic space need to compute only two sets

of characteristic variables adjacent to the cell interface instead of three sets of characteristic variables belonging to the entire stencil, the present method is more efficient than other limiting methods in terms of the characteristic variables. When extending the present method to multi-dimensional cases, this advantage will become more significant [46]. We note that the present limiting procedure is compact as it involves only the direct neighbors of the cell of interest.

4 Numerical results

Several one-dimensional benchmark test cases are solved to assess the accuracy, robustness and shock capturing capability of the CLSFV schemes. The temporal discretization is the classical fourth order Runge-Kutta scheme [63] (in the accuracy test for the scalar linear advection equation) or the third order TVD Runge-Kutta scheme (in all other test cases).

4.1 The scalar linear advection equation

The linear advection equation is solved to test the accuracy of the proposed schemes. The governing equation is

$$\frac{\partial u}{\partial t}+\frac{\partial u}{\partial x}=0$$

The initial condition is $u_0\left(x\right)=\sin\left(2\pi x\right)$. Periodic boundary conditions are imposed at the two end points of the region $0\le x\le 1$. The exact solution is $u\left(x,t\right)=u_0\left(x-t\right)$.The simulation is performed up to $t=1.0$ using a Courant number *CFL* =1.0. The errors of density in terms of L_1 and L_∞ norms and the rates of convergence are listed in Table 2.

Accuracy comparison among the schemes is shown in Fig. 5.

Table 2. Accuracy test results for the 1D linear advection equation.

Schemes	Grid	L_1 error	Order	L_∞ error	Order
Second order	20	3.34E-02		5.27E-02	
	40	8.27E-03	2.01	1.30E-02	2.02
	80	2.06E-03	2.01	3.23E-03	2.01
	160	5.14E-04	2.00	8.08E-04	2.00
	320	1.29E-04	2.00	2.02E-04	2.00
	640	3.21E-05	2.00	5.05E-05	2.00
Third order	20	1.02E-02		1.61E-02	
	40	1.29E-03	2.98	2.03E-03	2.99
	80	1.61E-04	3.00	2.54E-04	3.00
	160	2.02E-05	3.00	3.17E-05	3.00
	320	2.52E-06	3.00	3.96E-06	3.00
	640	3.15E-07	3.00	4.95E-07	3.00
Fourth order	20	3.10E-04		4.84E-04	
	40	9.83E-06	4.98	1.54E-05	4.97
	80	3.08E-07	4.99	4.84E-07	4.99
	160	9.64E-09	5.00	1.51E-08	5.00
	320	3.02E-10	5.00	4.74E-10	5.00

640	9.45E-12	5.00	1.48E-11	5.00

The results in Fig. 5 show that the second and third order schemes achieve the theoretical second-order and third-order accuracy. For the fourth order scheme, super convergence is observed and the rate of convergence is as large as 5.

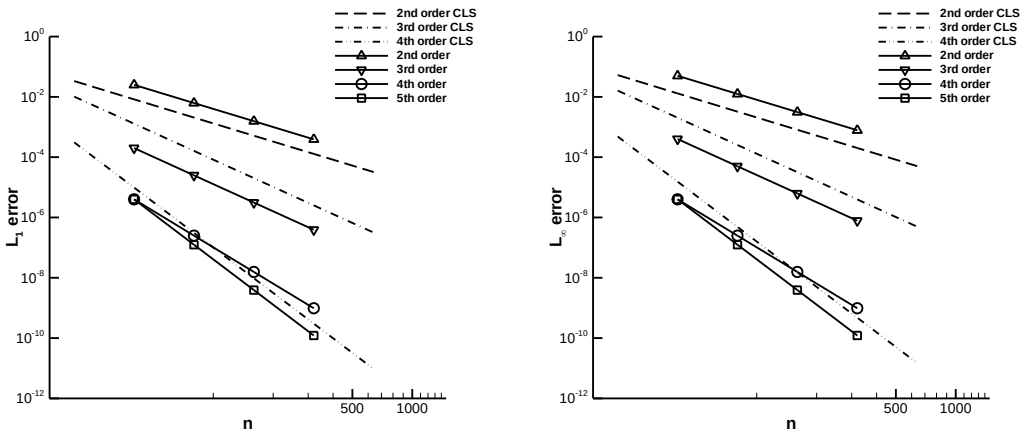

(a) L_1 error (b) L_∞ error

Fig. 5. The rate of convergence in terms of (a) L_1 norm and (b) L_∞ norm.

4.2 Propagation of broadband sound waves

This test problem describes the propagation of a sound wave packet which contains acoustic turbulent structures with various length scales. The initial conditions are

$$p(x,0) = p_0\left(1+\varepsilon\sum_{k=1}^{N/2}\left(E_p(k)\right)^{0.5}\sin\left(2\pi k\left(x+\psi_k\right)\right)\right),$$

$$\rho(x,0) = \rho_0\left(p(x,0)/p_0\right)^{1/\gamma},$$

$$u(x,0) = u_0 + \frac{2}{\gamma-1}\left(c(x,0)-c_0\right),$$

where

$$E_p(k) = (k/k_0)^4 e^{-2(k/k_0)^2}$$

is the energy spectrum which reaches its maximum at $k = k_0$. The computational domain is $x \in [0,1]$ and ψ_k is a random number ranging from 0 to 1. ε is a small parameter which determines the intensity of the acoustic turbulence and is chosen to be $\varepsilon = 0.001$ in the simulation. $c = \sqrt{\gamma p / \rho}$ is the speed of sound. Periodic boundary conditions are imposed at the boundaries. The computations are performed with different schemes for k_0 =4, 8, 12 on a *N* = 128 grid using a Courant number *CFL* = 0.2. The simulations are performed for one time period. When k_0 =4, most of the turbulent energy is concentrated at low wavenumbers, while for k_0 =12, the high wavenumber structures are more energetic. The numerical results in terms of the pressure distribution are shown in Figs. 6–8. When k_0 =4, all the schemes give very similar numerical results which means that all schemes can capture the low wavenumber flow features. However, as k_0 increases, the differences in resolution among the various schemes become more obvious. The fourth order scheme performs remarkably better than other schemes according to Fig. 7 and Fig. 8.

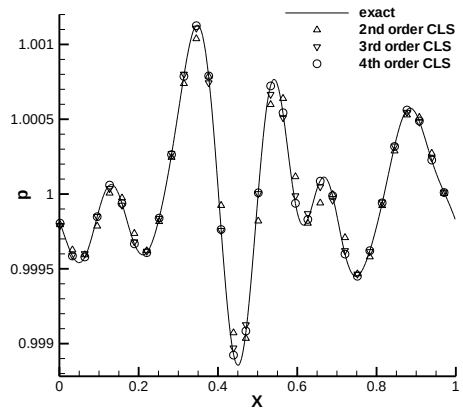

Fig. 6. Broadband wave propagation. Pressure distribution for the CLSFV schemes with k_0 = 4.

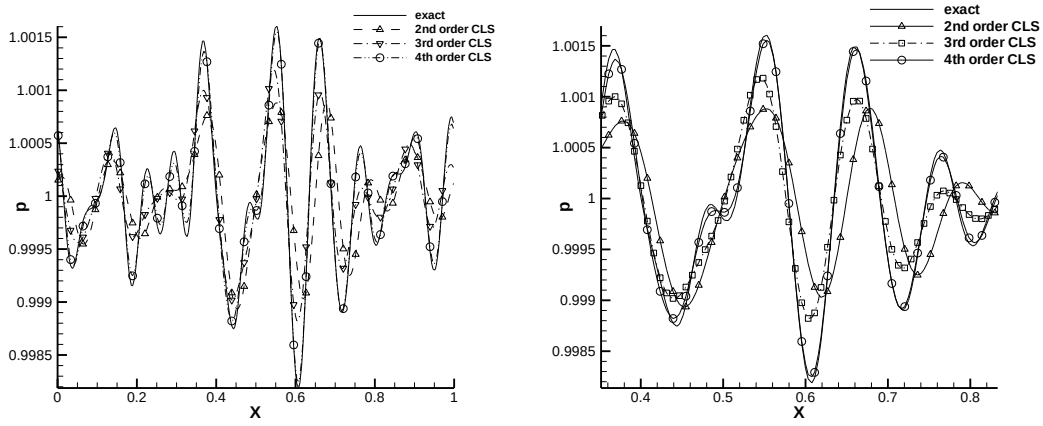

(b) Entire view (b) Enlargements

Fig. 7. Broadband wave propagation. Pressure distribution for the CLSFV schemes with $k_0 = 8$.

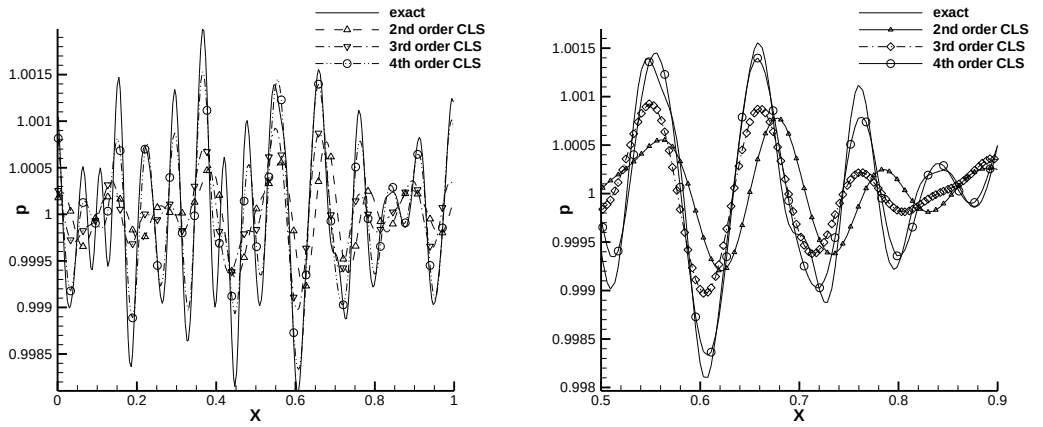

(a) Entire view (b) Enlargements

Fig. 8. Broadband wave propagation. Pressure distribution for the CLSFV schemes with $k_0 = 12$.

4.3 Sod problem [64]

This test case is a shock tube problem to test the capability of the second to fourth order CLSFV schemes with the WBAP limiter in capturing the strong shock wave and contact discontinuity. The initial distributions are defined as

$$(\rho_0, u_0, p_0) = \begin{cases} (1,0,1) & \text{for } 0 \le x \le 0.5 \\ (0.125,0,0.1) & \text{otherwise} \end{cases} \qquad (0 \le x \le 1).$$

The computations are performed with 200 cells until t = 0.25. The Courant number is *CFL*=1.0. This test uses the WBAP limiter and the successive limiting procedure in terms of the characteristic variables described in subsection 3.

The results of density distribution in Fig. 9 show that all the schemes can capture strong shock wave and contact discontinuity without oscillations. Furthermore, higher order scheme obtains result with higher resolution.

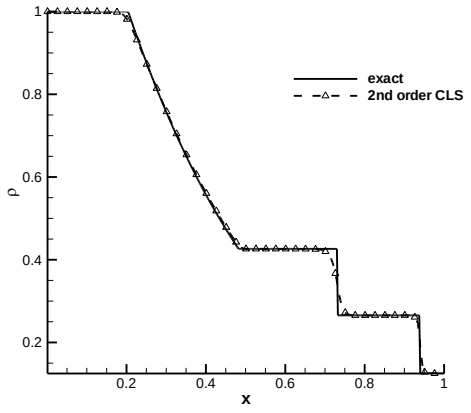

(a) Second order

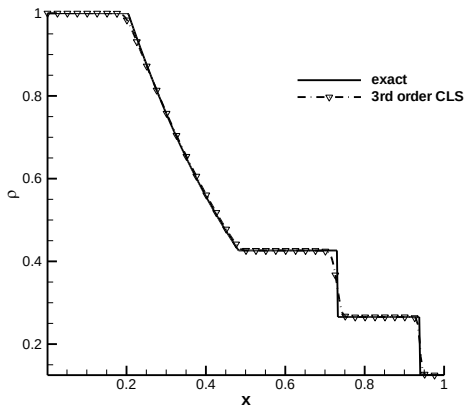

(b) Third order

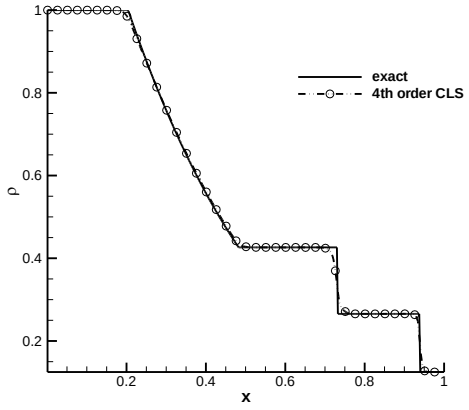

(c) Fourth order

Fig. 9. Sod problem. Density distribution at t = 0.25.

4.4 Lax problem [65]

Another well-known shock tube problem is the Lax problem. The initial conditions are

$$\left(\rho_0, u_0, p_0\right) = \begin{cases} \left(0.445, 0.698, 3.528\right) & \textit{for } 0 \le x \le 0.5 \\ \left(0.5, 0, 0.571\right) & \textit{otherwise} \end{cases} \qquad \left(0 \le x \le 1\right).$$

This problem is solved using the second to fourth order CLSFV schemes with the WBAP limiter. The computations are performed until t = 0.1 with 200 cells. The Courant number is *CFL*=1.0. The results of density distribution in Fig. 10 show that all the schemes give correct solutions with good resolution. According to Jiang and Shu [34], the Lax problem is a tough test case for non-characteristic-based schemes of order at least three. Oscillations can easily appear for such schemes. Therefore, the oscillation-free and high resolution solutions demonstrate the excellent shock capturing capability of the proposed schemes.

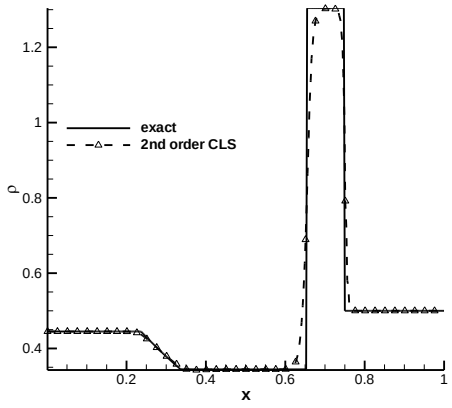

(a) Second order

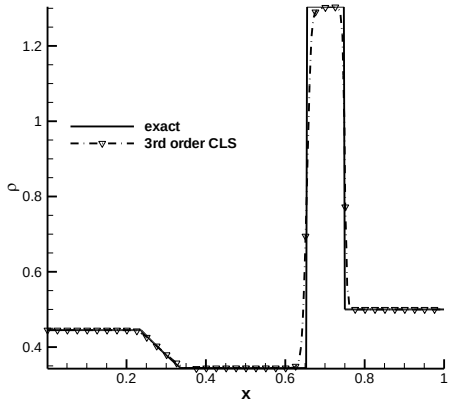

(b) Third order

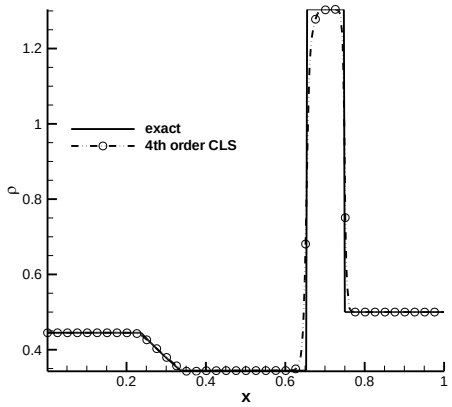

(c) Fourth order

Fig. 10. Lax problem. Density distribution at $t = 0.1$.

4.5 Two interacting blast waves [66]

This example is to simulate the interaction of two blast waves subjected to the initial conditions

$$(\rho, u, p) = \begin{cases} (1, 0, 1000) & for\ 0 \le x \le 0.1 \\ (1, 0, 0.01) & for\ 0.1 < x \le 0.9 \\ (1, 0, 100) & otherwise \end{cases}$$

on the computational domain [0,1] with 400 cells. Reflective boundary conditions are imposed at x=0 and x=1. This problem was discussed in detail in [66]. It is a severe numerical test case where discontinuity and shock wave are dominant.

The Courant number is CFL=1.0. The density distributions at t = 0.038 are shown in Fig. 11. The "exact" solution (solid line in the picture) is computed by the fifth order WENO scheme [34] with 2000 cells. The results of the third and fourth order schemes are much better than the second order scheme.

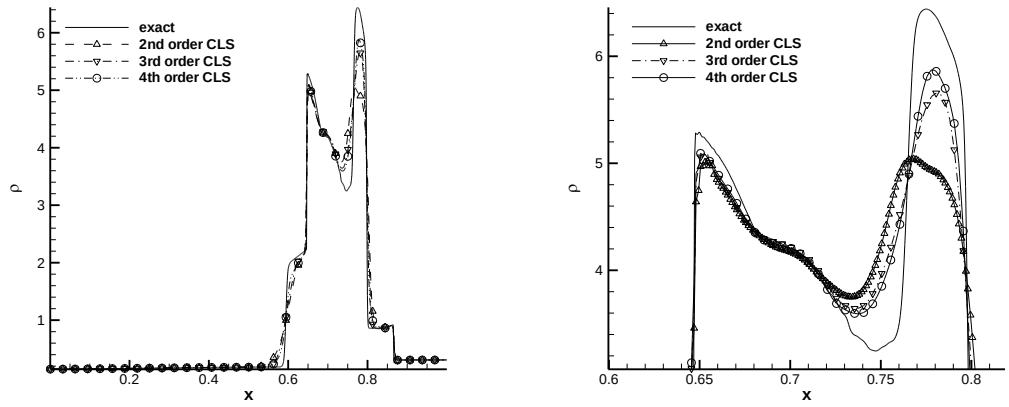

(a) Entire view (b) Enlargements

Fig. 11. Two interacting blast waves. Density distribution at t = 0.038.

4.6 Shu-Osher problem

This test case is to solve the Shu and Osher [33] problem which describes the interaction of an entropy sine wave with a Mach 3 right moving shock. The computational domain is [0, 10] and the initial conditions are

$$(\rho_0, u_0, p_0) = \begin{cases} (3.857143, 2.629369, 10.33333) & for\ 0 \le x < 1 \\ (1 + 0.2\sin(5x), 0, 1) & for\ x \ge 1 \end{cases}$$

Second to fourth order CLSFV schemes with the WBAP limiter are tested on a uniform grid with 500 cells. The computations are performed until t = 1.8 using a Courant number *CFL*=1.0. Since the exact solution of this problem is unknown, the numerical solution computed by the fifth order WENO scheme [34] using 20000 cells is taken as the exact solution. Figure 12 shows the density distributions. The results show that the solution of the fourth order scheme is rarely close to the exact solution and is better than the third order scheme which is, in turn, much better than the second order scheme. The results demonstrate the high resolution and excellent shock capturing capability of the CLSFV schemes.

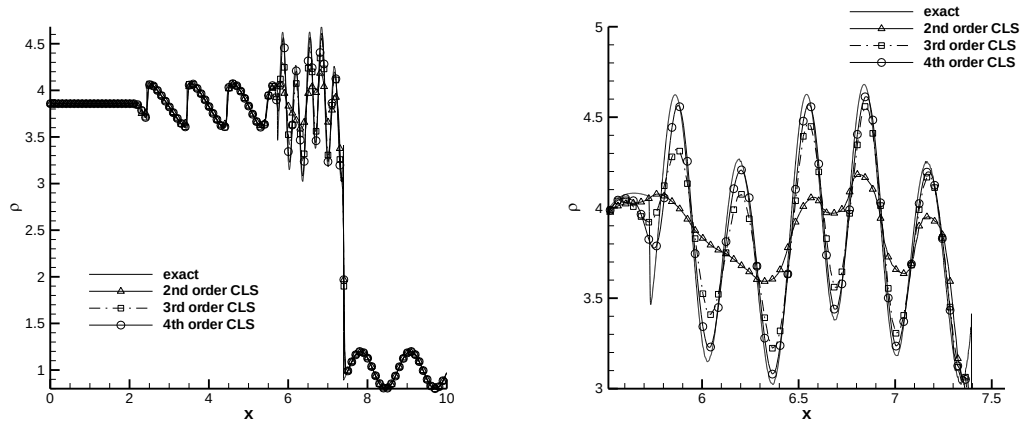

(a) Entire view (b) Enlargements

Fig. 12. Shu-Osher problem. Density distribution at t = 1.8.

5 Conclusions

This paper presents a CLS reconstruction procedure for high order FV method on unstructured grids. A set of constitutive relations are constructed by requiring the reconstruction polynomial and its spatial derivatives on the control volume of interest to conserve their averages on face-neighboring cells. These constitutive relations result in an over-determined linear equation system, which is solved using the least-squares method. This reconstruction procedure can achieve arbitrarily high order accuracy using a compact stencil involving only the face-neighbors. The Fourier analysis is presented to study the dispersion/dissipation and stability properties of the CLS reconstruction by applying it to the high order FV scheme for solving the scalar linear advection equation. Optimization of the dispersion property is performed to determine the optimal values of the free parameters in the reconstruction. The von-Neumann stability analysis shows that the second, third and fourth-order CLSFV schemes using the three-stage TVD Runge-Kutta time-stepping technique are stable up to a critical Courant number larger than 1. The CLSFV schemes are extended to solve the one-dimensional Euler equations. An improved WBAP limiter is proposed to efficiently suppress non-physical oscillations near discontinuities. The results of the benchmark test cases demonstrate the high order accuracy, robustness and shock capturing capability of the CLSFV method.

Acknowledgements

This work is supported by Projects U1430235 of NSFC.

References

[1] Zingg, D. W., De Rango, S., Nemec, M., & Pulliam, T. H. (2000). Comparison of several spatial discretizations for the Navier–Stokes equations. *Journal of computational Physics*, *160*(2), 683-704.

[2] Barth, T. J., & Frederickson, P. O. (1990). Higher order solution of the Euler equations on unstructured grids using quadratic reconstruction. *AIAA paper*, *90*, 0013.

[3] Delanaye, M., & Liu, Y. (1989). Quadratic Reconstruction Finite Volume Schemes on 3D Arbitrary Unstructured Polyhedral Grids. *AIAA paper*, *99*, 3259.

[4] Ollivier-Gooch, C., & Van Altena, M. (2002). A high-order-accurate unstructured mesh finite-volume scheme for the advection–diffusion equation. *Journal of Computational Physics*, *181*(2), 729-752.

[5] Ollivier-Gooch, C. F. (1997). Quasi-ENO schemes for unstructured meshes based on unlimited data-dependent least-squares reconstruction. *Journal of Computational Physics*, *133*(1), 6-17.

[6] Friedrich, O. (1998). Weighted essentially non-oscillatory schemes for the interpolation of mean values on unstructured grids. *Journal of Computational Physics*, *144*(1), 194-212.

[7] Dumbser, M., & Käser, M. (2007). Arbitrary high order non-oscillatory finite volume schemes on unstructured meshes for linear hyperbolic systems. *Journal of Computational Physics*, *221*(2), 693-723.

[8] Dumbser, M., Käser, M., Titarev, V. A., & Toro, E. F. (2007). Quadrature-free non-oscillatory finite volume schemes on unstructured meshes for nonlinear hyperbolic

systems. *Journal of Computational Physics*, *226*(1), 204-243.

[9] Hu, C., & Shu, C. W. (1999). Weighted essentially non-oscillatory schemes on triangular meshes. *Journal of Computational Physics*, *150*(1), 97-127.

[10] Reed, W. H., & Hill, T. R. (1973). Triangular mesh methods for the neutron transport equation. *Los Alamos Report LA-UR-73-479*.

[11] Cockburn, B., & Shu, C. W. (1989). TVB Runge-Kutta local projection discontinuous Galerkin finite element method for conservation laws. II. General framework. *Mathematics of Computation*, *52*(186), 411-435.

[12] Cockburn, B., Lin, S. Y., & Shu, C. W. (1989). TVB Runge-Kutta local projection discontinuous Galerkin finite element method for conservation laws III: one-dimensional systems. *Journal of Computational Physics*, *84*(1), 90-113.

[13] Cockburn, B., Hou, S., & Shu, C. W. (1990). The Runge-Kutta local projection discontinuous Galerkin finite element method for conservation laws. IV. The multidimensional case. *Mathematics of Computation*, *54*(190), 545-581.

[14] Cockburn, B., & Shu, C. W. (2001). Runge–Kutta discontinuous Galerkin methods for convection-dominated problems. *Journal of scientific computing*, *16*(3), 173-261.

[15] Dumbser, M., Balsara, D. S., Toro, E. F., & Munz, C. D. (2008). A unified framework for the construction of one-step finite volume and discontinuous Galerkin schemes on unstructured meshes. *Journal of Computational Physics*, *227*(18), 8209-8253.

[16] Dumbser, M. (2010). Arbitrary high order P_NP_M schemes on unstructured meshes for the compressible Navier–Stokes equations. *Computers & Fluids*, *39*(1), 60-76.

[17] Dumbser, M., & Zanotti, O. (2009). Very high order P_NP_M schemes on unstructured

meshes for the resistive relativistic MHD equations. *Journal of Computational Physics*, *228*(18), 6991-7006.

[18]Abgrall, R., & Mezine, M. (2003). Construction of second order accurate monotone and stable residual distribution schemes for unsteady flow problems. *Journal of Computational Physics*, *188*(1), 16-55.

[19]Ricchiuto, M., Csík, Á., & Deconinck, H. (2005). Residual distribution for general time-dependent conservation laws. *Journal of Computational Physics*, *209*(1), 249-289.

[20]Abgrall, R. (2006). Residual distribution schemes: current status and future trends. *Computers & Fluids*, *35*(7), 641-669.

[21]Abgrall, R., Larat, A., & Ricchiuto, M. (2011). Construction of very high order residual distribution schemes for steady inviscid flow problems on hybrid unstructured meshes. *Journal of Computational Physics*, *230*(11), 4103-4136.

[22]Wang, Z. J. (2002). Spectral (finite) volume method for conservation laws on unstructured grids: basic formulation: Basic formulation. *Journal of Computational Physics*, *178*(1), 210-251.

[23]Wang, Z. J., & Liu, Y. (2002). Spectral (finite) volume method for conservation laws on unstructured grids: II. Extension to two-dimensional scalar equation. *Journal of Computational Physics*, *179*(2), 665-697.

[24]Wang, Z. J., & Liu, Y. (2004). Spectral (finite) volume method for conservation laws on unstructured grids III: One dimensional systems and partition optimization. *Journal of Scientific Computing*, *20*(1), 137-157.

[25]Wang, Z. J., Zhang, L., & Liu, Y. (2004). Spectral (finite) volume method for

conservation laws on unstructured grids IV: extension to two-dimensional systems. *Journal of Computational Physics*, *194*(2), 716-741.

[26]Liu, Y., Vinokur, M., & Wang, Z. J. (2006). Spectral difference method for unstructured grids I: basic formulation. *Journal of Computational Physics*, *216*(2), 780-801.

[27]Wang, Z. J., Liu, Y., May, G., & Jameson, A. (2007). Spectral difference method for unstructured grids II: extension to the Euler equations. *Journal of Scientific Computing*, *32*(1), 45-71.

[28]May, G., & Jameson, A. (2006). A spectral difference method for the Euler and Navier-Stokes equations on unstructured meshes. *AIAA paper*, *304*, 2006.

[29]Wang, Z. J., & Gao, H. (2009). A unifying lifting collocation penalty formulation including the discontinuous Galerkin, spectral volume/difference methods for conservation laws on mixed grids. *Journal of Computational Physics*, *228*(21), 8161-8186.

[30]Huynh, H. T. (2007). A flux reconstruction approach to high-order schemes including discontinuous Galerkin methods. *AIAA paper*, *4079*, 2007.

[31]Harten, A., Engquist, B., Osher, S., & Chakravarthy, S. R. (1987). Uniformly high order accurate essentially non-oscillatory schemes, III. *Journal of computational physics*, *71*(2), 231-303.

[32]Shu, C. W., & Osher, S. (1988). Efficient implementation of essentially non-oscillatory shock-capturing schemes. *Journal of Computational Physics*,*77*(2), 439-471.

[33]Shu, C. W., & Osher, S. (1989). Efficient implementation of essentially non-oscillatory shock-capturing schemes, II. *Journal of Computational Physics*, *83*(1), 32-78.

[34]Jiang, G. S., & Shu, C. W. (1996). Efficient implementation of weighted ENO schemes. *Journal of computational physics*, *126*(1), 202-228.

[35]Balsara, D. S., & Shu, C. W. (2000). Monotonicity preserving weighted essentially non-oscillatory schemes with increasingly high order of accuracy. *Journal of Computational Physics*, *160*(2), 405-452.

[36]Henrick, A. K., Aslam, T. D., & Powers, J. M. (2006). Simulations of pulsating one-dimensional detonations with true fifth order accuracy. *Journal of Computational Physics*, *213*(1), 311-329.

[37]Borges, R., Carmona, M., Costa, B., & Don, W. S. (2008). An improved weighted essentially non-oscillatory scheme for hyperbolic conservation laws. *Journal of Computational Physics*, *227*(6), 3191-3211.

[38]Balsara, D. S., Rumpf, T., Dumbser, M., & Munz, C. D. (2009). Efficient, high accuracy ADER-WENO schemes for hydrodynamics and divergence-free magnetohydrodynamics. *Journal of Computational Physics*, *228*(7), 2480-2516.

[39]Balsara, D. S. (2009). Divergence-free reconstruction of magnetic fields and WENO schemes for magnetohydrodynamics. *Journal of Computational Physics*, *228*(14), 5040-5056.

[40]Abgrall, R. (1994). On essentially non-oscillatory schemes on unstructured meshes: analysis and implementation. *Journal of Computational Physics*, *114*(1), 45-58.

[41]Li, W., & Ren, Y. X. (2012). High-order k-exact WENO finite volume schemes for solving gas dynamic Euler equations on unstructured grids. *International Journal for Numerical Methods in Fluids*, *70*(6), 742-763.

[42]Zhang, L., Liu, W., He, L., Deng, X., & Zhang, H. (2012). A class of hybrid DG/FV methods for conservation laws I: Basic formulation and one-dimensional systems. *Journal of Computational Physics*, *231*(4), 1081-1103.

[43]Batista, M. (2006). A cyclic block-tridiagonal solver. *Advances in Engineering Software*, *37*(2), 69-74.

[44]Li, W., & Ren, Y. X. (2012). The multi-dimensional limiters for solving hyperbolic conservation laws on unstructured grids II: extension to high order finite volume schemes. *Journal of Computational Physics*, *231*(11), 4053-4077.

[45]Zhong, X., & Shu, C. W. (2013). A simple weighted essentially nonoscillatory limiter for Runge–Kutta discontinuous Galerkin methods.*Journal of Computational Physics*, *232*(1), 397-415.

[46]Li, W., & Ren, Y. X. (2014). The multi-dimensional limiters for discontinuous Galerkin method on unstructured grids. *Computers & Fluids*, *96*, 368-376.

[47]Lele, S. K. (1992). Compact finite difference schemes with spectral-like resolution. *Journal of computational physics*, *103*(1), 16-42.

[48]Tam, C. K., & Webb, J. C. (1993). Dispersion-relation-preserving finite difference schemes for computational acoustics. *Journal of computational physics*, *107*(2), 262-281.

[49]Zhong, X. (1998). High-order finite-difference schemes for numerical simulation of hypersonic boundary-layer transition. *Journal of Computational Physics*, *144*(2), 662-709.

[50]Deng, X., & Zhang, H. (2000). Developing high-order weighted compact nonlinear schemes. *Journal of Computational Physics*, *165*(1), 22-44.

[51]Liu, X., Zhang, S., Zhang, H., & Shu, C. W. (2013). A new class of central compact schemes with spectral-like resolution I: Linear schemes. *Journal of Computational Physics*, *248*, 235-256.

[52]Chu, P. C., & Fan, C. (1998). A three-point combined compact difference scheme. *Journal of Computational Physics*, *140*(2), 370-399.

[53]Shen, M. Y., Zhang, Z. B., & Niu, X. L. (2003). A new way for constructing high accuracy shock-capturing generalized compact difference schemes. *Computer methods in applied mechanics and engineering*, *192*(25), 2703-2725.

[54]Pereira, J. M. C., Kobayashi, M. H., & Pereira, J. C. F. (2001). A fourth-order-accurate finite volume compact method for the incompressible Navier–Stokes solutions. *Journal of Computational Physics*, *167*(1), 217-243.

[55]Lacor, C., Smirnov, S., & Baelmans, M. (2004). A finite volume formulation of compact central schemes on arbitrary structured grids. *Journal of Computational Physics*, *198*(2), 535-566.

[56]Elhami Amiri, A., Kazemzadeh Hannani, S., & Mashayek, F. (2005). Evaluation of a fourth-order finite-volume compact scheme for LES with explicit filtering. *Numerical Heat Transfer, Part B: Fundamentals*, *48*(2), 147-163.

[57]Fosso, A., Deniau, H., Sicot, F., & Sagaut, P. (2010). Curvilinear finite-volume schemes using high-order compact interpolation. *Journal of Computational Physics*, *229*(13), 5090-5122.

[58]Mart ń, M. P., Taylor, E. M., Wu, M., & Weirs, V. G. (2006). A bandwidth-optimized WENO scheme for the effective direct numerical simulation of compressible turbulence.

Journal of Computational Physics, *220*(1), 270-289.

[59]Li, W., Ren, Y. X., Lei, G., & Luo, H. (2011). The multi-dimensional limiters for solving hyperbolic conservation laws on unstructured grids. *Journal of Computational Physics*, *230*(21), 7775-7795.

[60]Roe, P. L. (1981). Approximate Riemann solvers, parameter vectors, and difference schemes. *Journal of computational physics*, *43*(2), 357-372.

[61]Harten, A. (1983). High resolution schemes for hyperbolic conservation laws. *Journal of computational physics*, *49*(3), 357-393.

[62]Sweby, P. K. (1984). High resolution schemes using flux limiters for hyperbolic conservation laws. *SIAM journal on numerical analysis*, *21*(5), 995-1011.

[63]Jameson, A., Schmidt, W., & Turkel, E. (1981). Numerical solutions of the Euler equations by finite volume methods using Runge-Kutta time-stepping schemes. *AIAA paper*, *1259*, 1981.

[64]Sod, G. A. (1978). A survey of several finite difference methods for systems of nonlinear hyperbolic conservation laws. *Journal of computational physics*, *27*(1), 1-31.

[65]Lax, P. D. (1954). Weak solutions of nonlinear hyperbolic equations and their numerical computation. *Communications on pure and applied mathematics*, *7*(1), 159-193.

[66]Woodward, P., & Colella, P. (1984). The numerical simulation of two-dimensional fluid flow with strong shocks. *Journal of Computational Physics*, *54*(1), 115-173.